

Mie Resonance Enhancement of Laser Cooling in Rare-Earth Doped Materials

GALINA NEMOVA^{1,*} AND CHRISTOPHE CALOZ^{1,2}

¹*Polytechnique Montréal, 2500 ch. de Polytechnique, Montréal, H3T 1J4, QC, Canada.*

²*KU Leuven, Kasteelpark Arenberg 10, box 2444, 3001 Leuven, Belgium.*

*Corresponding author: galina.nemova@videotron.ca

Laser cooling of solids keeps attracting attention owing to a broad range of its applications that extends from *cm*-sized all-optical cryocoolers for airborne and space-based applications to cooling on *nanoparticles* for biological and mesoscopic physics. Laser cooling of nanoparticles is a challenging task. We propose to use Mie resonances to enhance anti-Stokes fluorescence laser cooling in rare-earth (RE) doped nanoparticles made of low-phonon glasses or crystals. As an example, we consider an Yb³⁺:YAG nanosphere pumped at the long wavelength tail of the Yb³⁺ absorption spectrum at 1030 nm. We show that if the radius of the nanosphere is adjusted to the pump wavelength in such a manner that the pump excites some of its Mie resonant modes, the cooling power density generated in the sample is considerably enhanced and the temperature of the sample is consequently considerably (~ 63%) decreased. This concept can be extended to nanoparticles of different shapes and made from different low-phonon RE doped materials suitable for laser cooling by anti-Stokes fluorescence.

I. INTRODUCTION

In 1929, Peter Pringsheim proposed the idea to cool sodium vapor with light using anti-Stokes fluorescence [1]. This idea was based on experimental evidence that some materials emit light at shorter wavelength than the material illumination wavelength. The source of this quantum defect was inelastic collisions of sodium atoms that is thermalization. Light cooling in solids by anti-Stokes fluorescence was realized only in 1995, by Richard Epstein and colleagues [2]. They experimentally demonstrated a drop of the temperature of a *cm*-sized ytterbium-doped fluorozirconate ZrF₄-BaF₂-LaF₃-AlF₃-NaF-PbF₂ (ZBLANP) glass sample by 0.3 K below room temperature. This success was largely owed to the recent development of high-quality ZBLANP for the telecommunication industry and of coherent light sources (lasers).

Since its first experimental demonstration by Epstein, laser cooling of solids via anti-Stokes fluorescence has been realized with different rare-earth (RE) ions, including Yb³⁺, Er³⁺, Tm³⁺ and Ho³⁺ ions, doped in a wide variety of low-phonon glasses and crystals [3–8]. The ytterbium (Yb³⁺) ions have eventually been found to represent the best choice for laser cooling applications. Indeed, ytterbium has only one excited manifold, and it therefore is free from excited state absorption, which is a source of undesirable non-radiative decay that results in heat generation. A record low temperature of ~ 91 K has been achieved in an Yb³⁺:YLF sample [9, 10].

The technology of laser cooling by anti-Stokes fluorescence has numerous applications. For example, it can be used for development of a solid-state all-optical cryocoolers, which are based on *cm*-sized RE-doped low-phonon crystal or glass samples. Such all-optical cryocoolers are compact, reliable, and free from vibrations and moving parts or fluids devices. They can be used for the cryogenic refrigeration of

semiconductor devices in applications with tight weight and size constraints, such as airborne and space-based detector systems. The first all-solid-state optical cryocooler was demonstrated in 2018 [11].

Laser cooling by anti-Stokes fluorescence can also be realized in radiation-balanced solid-state bulk lasers where the heat generated by the quantum defect between the pump and laser signals is offset by cooling from anti-Stokes emission [12]. This technology can be used for mitigating heat generation in disc lasers [13, 14]. Specifically, researchers proposed the idea to cool an RE-doped fiber laser cladding with anti-Stokes fluorescence to mitigate heat generated in the RE-doped fiber laser core during the amplification process [15], this proposal was experimentally demonstrated in [16, 17].

The size and shape of the laser cooled sample as well as RE ion concentration in this sample are important parameters in the optimization of the laser cooling process [18]. In the recent years, interest has emerged in the laser cooling of small, *μm*- and *nm*-sized RE-doped samples [19–21]. Such small samples are of interest for biological applications and mesoscopic physics. However, laser cooling at the nanoscale is not an easy task [18].

In this paper, we propose an approach to enhance the laser cooling process in RE-doped nanospheres with a diameter of a few hundreds of nanometers. Our approach is based on optimization of the sample size by leveraging the Mie resonance concept and theory [22]. As an example, an Yb³⁺:YAG nanosphere pumped at the wavelength $\lambda_p = 1030$ nm located in the long wavelength tail of the Yb³⁺ absorption spectrum is considered (Fig. 1). The mean fluorescence wavelength of the spontaneous radiation $\lambda_F < \lambda_p$. A bulk Yb³⁺:YAG sample was laser cooled in [23]. Section II describes the theory of laser cooling in bulk and nanosphere samples. Section III presents and discusses the results. Conclusions are given in Sec. IV.

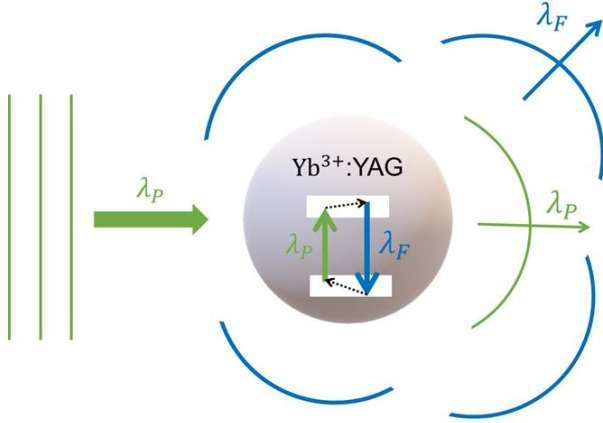


Fig. 1 Nanosphere system under investigation. Here λ_P and λ_F are the pump and mean fluorescence wavelengths, respectively.

II. THEORETICAL ANALYSIS

A. Laser Cooling in Yb³⁺:YAG

The process of laser cooling with anti-Stokes fluorescence of RE-doped samples has been considered in details in a number of works [6, 8, 18]. Here we only briefly discuss this process. It is well known that the energy levels of RE ions doped in a host material undergo splitting as a result of the Stark effect. In the case of Yb³⁺:YAG samples two energy levels $^2F_{7/2}$ and $^2F_{5/2}$ of Yb³⁺ ions split into four and three sublevels, respectively (Fig. 2a). It is worth to remind that YAG (yttrium aluminum garnet) is one of the most widely used optical materials in laser physics and laser cooling of solids, due to its high thermal stability, good chemical resistance, and low-phonon energy. In thermal equilibrium, the population of each sublevel is described by the Boltzmann distribution. This thermal equilibrium can be reached via phonon absorption and phonon emission. Indeed, each electron at each sublevel of the ions interact with phonons of the host material by absorbing phonons at the rate A_{NR}^+ or emitting phonons at the rate A_{NR}^- , as shown in Fig. 2a. This process, known as the thermalization, takes place at the ps -time scale.

Let us consider a laser cooling cycle in Yb³⁺:YAG. It includes phonon absorption at the wavelength λ_P , thermalization in the excited $^2F_{5/2}$ manifold accompanied by phonon absorption, and spontaneous photon emission from the excited $^2F_{5/2}$ manifold to the ground $^2F_{7/2}$ manifold. All photon absorption-emission cycles where the energy of the radiated photon exceeds the energy of the absorbed one (anti-Stokes fluorescence) result in cooling, since this energy difference has to be compensated by phonon absorption. All the photon absorption-emission cycles where the energy of the absorbed photons exceeds the energy of the radiated ones (Stokes fluorescence) causes heat generation in the sample,

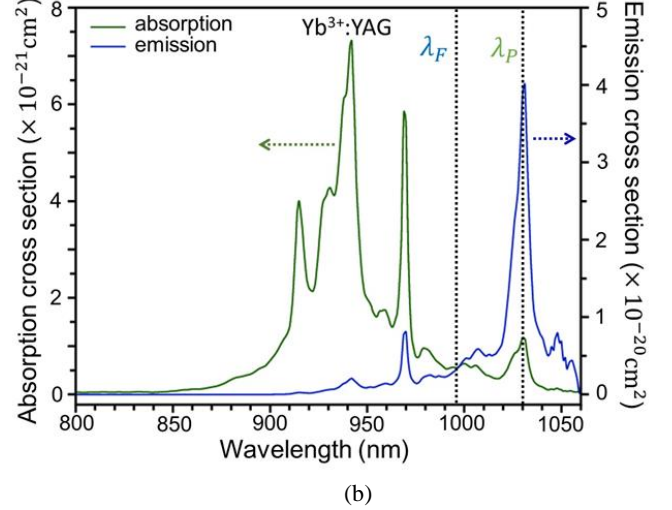
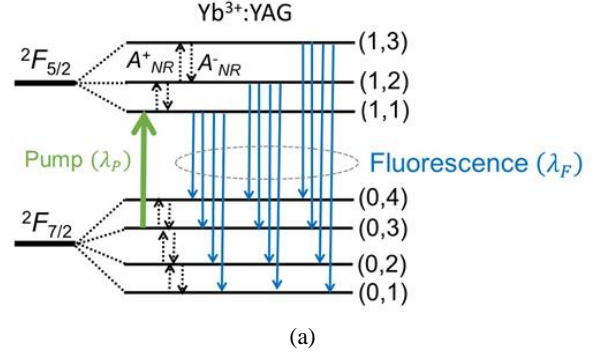


Fig. 2 Spectroscopy of the Yb³⁺:YAG sample. (a) Energy levels. (b) Absorption and emission cross sections versus wavelength.

since the energy difference in these cycles has to be compensated by phonon generation (Fig. 2a).

Spontaneous emission is characterized by the mean fluorescence frequency

$$\nu_F = \frac{\int \Phi(\nu) \nu d\nu}{\int \Phi(\nu) d\nu}, \quad (1)$$

where $\Phi(\nu)$ is the fluorescence flux density, which can be obtained experimentally, and $\nu_F = c/\lambda_F$. Here λ_F is the mean fluorescence wavelength and c is the speed of light in vacuum. If one wants to cool a sample, the pump wavelength, λ_P , has to exceed the mean fluorescence wavelength, λ_F , and all radiated photons with wavelengths smaller than λ_F must leave the sample (not to be reabsorbed by Yb³⁺ ions). Indeed, these short-wavelength reabsorbed photons serve as the source of heat generation in the sample, which is undesirable for cooling. The efficiency of the cooling cycle can be estimated as the difference between the energies of the anti-Stokes emitted photon and the pump photon normalized by the energy of the pump photon that is

$$\eta_{cool} = \frac{h\nu_F - h\nu_P}{h\nu_P} = \frac{\lambda_P}{\lambda_F} - 1. \quad (2)$$

The electrons excited to the $^2F_{5/2}$ manifold can also decay nonradiatively to the ground $^2F_{7/2}$ manifold generating phonons. The ‘‘competition’’ between the radiative and nonradiative decays of the $^2F_{5/2}$ electrons can be quantified by the quantum efficiency

$$\eta_q = \frac{W_r}{W_r + W_{nr}} \quad (3)$$

where $W_r = 1/\tau_r$ and $W_{nr} = 1/\tau_{nr}$ are the radiative and nonradiative decay rates, respectively, with τ_r and τ_{nr} being the radiative and nonradiative lifetimes of the excited manifold, respectively. We consider only high-quality $\text{Yb}^{3+}:\text{YAG}$ samples with the quantum efficiency as high as $\eta_q \geq 99\%$. Only such samples are suitable for laser cooling. Indeed, in this case the probability of nonradiative decay with phonon generation from the excited $^2F_{5/2}$ to the ground $^2F_{7/2}$ manifold is very low [8].

The strength of the pump absorption process can be quantified by the absorption cross section (Fig. 2b), which can be obtained experimentally. For example, if the intensity of the pump source at the wavelength λ_p is $I_p(\lambda_p)$, the number of photons absorbed per unit volume of the RE-doped sample per second is $N_T \sigma_a(\lambda_p) I_p(\lambda_p) / (h\nu_p)$, where N_T is the RE-ion concentration in the sample, h is the Planck constant, $\nu_p = c/\lambda_p$ is the pump photon frequency. The cooling power generated in the sample, P_{cool} , can be estimated as the difference between the absorbed and radiated powers. In the steady-state regime the cooling power generated in the sample with the volume V is [6]

$$P_{cool} = \frac{h\tilde{\nu}_F - h\nu_p}{h\nu_p} \frac{VN_T \sigma_a(\nu_p) I_p}{\left[1 + \frac{I_p}{I_S} \left(1 + \frac{\sigma_e(\nu_p)}{\sigma_a(\nu_p)}\right)\right]} \approx \frac{h\tilde{\nu}_F - h\nu_p}{h\nu_p} VN_T \sigma_a(\nu_p) I_p, \quad (4)$$

where $I_S = h\nu_p / [\eta_q \tau_r \sigma_a(\nu_p)]$ is the saturation intensity and $\tilde{\nu}_F = (2\eta_q - 1)\nu_F \approx \eta_q \nu_F$ is the effective mean fluorescence frequency. If the sample is placed on a low-contact and low-thermal conductivity support in a vacuum chamber, only radiative heat load may take place in the system. The final equilibrium temperature of the sample, T_s , can then be estimated by the Stefan-Boltzmann law,

$$P_{cool} = \varepsilon \sigma_B S (T_r^4 - T_s^4), \quad (5)$$

where S is the total surface area of the sample, T_r is room temperature, and ε is the sample emissivity. As one can understand from (2), the efficiency of laser cooling cycles is very low (a few %). Enhancement of the laser cooling process is therefore highly desirable.

B. Mie Resonance Cooling

Let us consider the laser cooling process in a $\text{Yb}^{3+}:\text{YAG}$ nanosphere pumped with a plane electromagnetic wave propagating in vacuum at the pump wavelength λ_p (Fig. 1).

According to Mie theory, the pump plane wave can be expanded in spherical harmonics as

$$\vec{E}_p = E_0 \sum_{n=1}^{\infty} i^n \frac{2n+1}{n(n+1)} [\vec{M}_{o1n}^{(1)} - i\vec{N}_{e1n}^{(1)}], \quad (6)$$

where E_0 is the amplitude of the incident field, \vec{M}_{o1n} and \vec{N}_{e1n} are the vector spherical harmonics

$$\begin{aligned} \vec{M}_{o1n}^{(1)} &= \cos\varphi \cdot \pi_n(\cos\theta) \cdot j_n(\tilde{r}) \hat{e}_\theta - \sin\varphi \cdot \\ &\quad \tau_n(\cos\theta) j_n(\tilde{r}) \hat{e}_\varphi, \end{aligned} \quad (7)$$

$$\begin{aligned} \vec{N}_{e1n}^{(1)} &= n(n+1) \cos\varphi \cdot \sin\theta \cdot \pi_n(\cos\theta) \cdot \frac{j_n(\tilde{r})}{\tilde{r}} \hat{e}_r + \cos\varphi \cdot \\ &\quad \tau_n(\cos\theta) \frac{[\tilde{r} j_n(\tilde{r})]'}{\tilde{r}} \hat{e}_\theta - \sin\varphi \cdot \pi_n(\cos\theta) \frac{[\tilde{r} j_n(\tilde{r})]'}{\tilde{r}} \hat{e}_\varphi, \end{aligned}$$

where $\tilde{r} = 2\pi n_{yb} r / \lambda_p$ and r is the radial distance. The index $n = 1$ stands for dipole, $n = 2$ quadrupole, etc., j_n are the spherical Bessel functions, and π_n and τ_n are the angle-dependent functions defined as

$$\pi_n = \frac{P_n^1}{\sin\theta}, \text{ and } \tau_n = \frac{dP_n^1}{d\theta}, \quad (8)$$

where P_n^1 is the associated Legendre function of first kind of degree n and the first order. The field inside the sphere reads [22, 24]

$$\vec{E} = E_0 \sum_{n=1}^{\infty} i^n \frac{2n+1}{n(n+1)} [c_n \vec{M}_{o1n}^{(1)} - i d_n \vec{N}_{e1n}^{(1)}], \quad (9)$$

where the coefficients c_n and d_n are functions of the normalized radius of the sphere, $x = 2\pi R / \lambda_p$, with R being the radius of the sphere, and read

$$c_n = \frac{j_n(x) [x h_n^{(1)}(x)]' - h_n^{(1)}(x) [x j_n(x)]'}{j_n(mx) [x h_n^{(1)}(x)]' - h_n^{(1)}(x) [m x j_n(mx)]'}, \quad (10)$$

$$d_n = \frac{m j_n(x) [x h_n^{(1)}(x)]' - m h_n^{(1)}(x) [x j_n(x)]'}{m^2 j_n(mx) [x h_n^{(1)}(x)]' - h_n^{(1)}(x) [m x j_n(mx)]'}, \quad (11)$$

where $h_n^{(1)}$ is the spherical Hankel functions, $m = n_{yb}$. The c_n coefficients describe the magnetic multipole modes and the d_n coefficients describe the electric multipole modes. At values of R for which the denominator of c_n coefficient or the denominator of d_n vanishes, the sphere resonates and scattering exhibits therefore a peak that dominates the response of the sphere. The radial dependence of the absolute-square of the electric field averaged over polar angle, θ , and azimuthal angle, φ , of spherical coordinates has the form

$$\langle |\vec{E}|^2 \rangle = \frac{E_0^2}{4} \sum_{n=1}^{\infty} (m_n |c_n|^2 + n_n |d_n|^2), \quad (12)$$

where m_n and n_n are functions of the radial distance, r , and are given as

$$m_n = 2(2n + 1)|j_n(\tilde{r})|^2, \quad (13)$$

$$n_n = 2n(2n + 1) \left[(n + 1) \left| \frac{j_n(\tilde{r})}{\tilde{r}} \right|^2 + \left| \frac{(\tilde{r} \cdot j_n(\tilde{r}))'}{\tilde{r}} \right|^2 \right], \quad (14)$$

where $\tilde{r} = 2\pi n_{Yb} r / \lambda_p$.

The cooling power generated in the sphere can be estimated as the difference between the pump power absorbed by the Yb^{3+} ions in the sphere and the power radiated with anti-Stokes fluorescence at the mean fluorescence wavelength. The field intensity given by (12) can then be integrated over the nanosphere and then inserted into (4) as

$$P_{cool} = 4\pi \left(\frac{h\nu_F - h\nu_P}{h\nu_P} \right) N_T \sigma_a(\nu_P) \sqrt{\frac{\epsilon_0}{\mu_0}} \int_0^R \langle |\vec{E}|^2 \rangle r^2 dr, \quad (15)$$

which corresponds to the cooling power generated in the Mie-resonant nanosphere.

III. RESULTS AND DISCUSSION

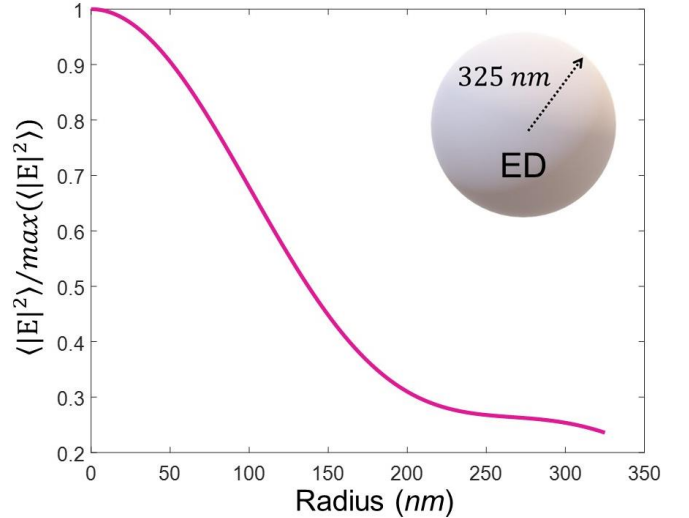
Let us consider an RE-doped nanosphere with radius of a few hundred nanometers. The energy levels of Yb^{3+} ions in a bulk Yb^{3+} :YAG sample, shown in Fig. 2a, remain essentially unchanged when the size of the sample is reduced to a few hundred nanometers. Moreover, phonon quantization, which can affect the thermalization process in the RE-doped nanocrystal, is inessential in such samples. We consider, as an example, a sample with ion concentration of $\sim 10\%$, which is smaller than the critical concentration of Yb^{3+} :YAG (17%). Such samples are free from cooperative effects such as resonant-radiative transfer (reabsorption), resonant nonradiative transfer and so on, which deteriorate laser cooling [6]. Indeed, these cooperative effects result to the

excited energy migration from the ion to ion inside the sample. This migrating energy can excite impurities in the sample and decay nonradiatively causing heat generation in the sample. The pump power considered in all our simulations is $I_p = 0.5 \cdot 10^{-4} W/\mu m^2$. Physical properties and parameters of Yb^{3+} :YAG samples used in our simulations are summarized in Table 1.

As one can see in relations (5), the temperature of the sample depends on the cooling power generated in the sample. The cooling power generated in the nanosphere can be estimated with relation (15), which depends on the electric field intensity distribution, $\langle |\vec{E}|^2 \rangle$, inside the sample. This distribution depends on the Mie resonant modes. Let us consider Mie modes of spheres with different radii. As may be seen in (10, 11), if the c_n coefficient exhibits a peak, a magnetic multipole mode dominates the response of the sphere, while if the d_n coefficient exhibits a peak, an electric multipole mode dominates the sphere. These coefficients exhibit peaks when their denominators tend to zero. For each n , there are several radii for which the denominators of c_n and d_n tend to zero. For example, at the pump wavelength $\lambda_p = 1030 nm$ the magnetic dipole (MD) mode ($n = 1$) can be supported by the sphere with the resonant radius $\sim 200 nm$ or $\sim 485 nm$, the magnetic quadrupole (MQ) modes ($n = 2$) can be supported by the sphere with the resonant radius $\sim 312 nm$ or $\sim 600 nm$. The electric dipole (ED) mode ($n = 1$) can be supported by the sphere with the resonant radius $\sim 325 nm$; and the electric quadrupole (EQ) mode ($n = 2$) can be supported by the sphere with the resonant radius $\sim 423 nm$. The absolute-square of the electric field averaged over polar angle, θ , and azimuthal angle, φ , of spherical coordinates, $\langle |\vec{E}|^2 \rangle$, for the ED mode of the sphere with the resonant radius $\sim 325 nm$ and for the MQ mode of the sphere with the resonant radius $\sim 312 nm$ is presented in Fig. 3. These field distributions have been simulated with relation (12).

Table 1. Physical properties of YAG and Yb^{3+} :YAG

YAG	
Crystal structure	cubic
Density ($g \cdot cm^{-3}$)	4.56
Thermal expansion (C^{-1})	7.8×10^{-6}
Thermal conductivity ($W \cdot m^{-1} \cdot C^{-1}$)	13
Refractive index	1.83
Phonon energy (cm^{-1})	~ 630
Yb^{3+} :YAG	
λ_p (nm)	1030
$\sigma_a(\lambda_p)$ (cm^2)	1.25×10^{-21}
$\sigma_e(\lambda_p)$ (cm^2)	4×10^{-20}
τ_r (μs)	~ 951
N_T	10%
Critical Yb^{3+} concentration (ions/ cm^3)	2.3×10^{21}



(a)

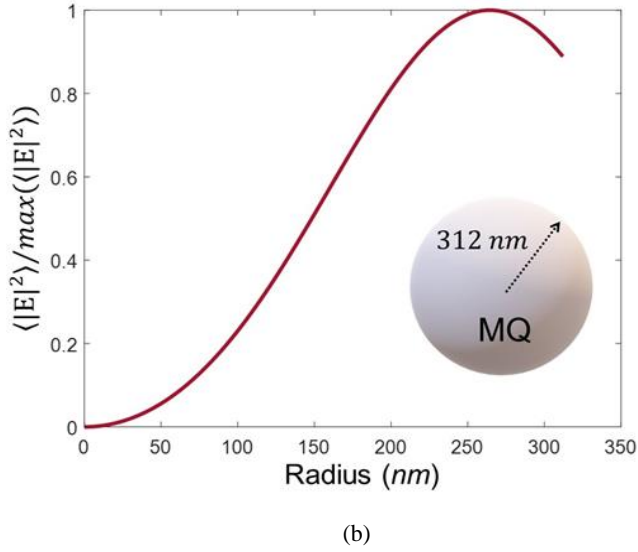


Fig. 3. Distribution of the squared modulus of the electric field averaged over the polar angle, θ , and the azimuthal angle, φ , along the radius of the sphere. (a) Electric dipole mode in the sphere with the radius $R \approx 325 \text{ nm}$. (b) Magnetic quadrupole mode in the sphere with the radius $R \approx 312 \text{ nm}$. These results have been computed using (12).

The cooling power density generated in the nanosphere, $\rho_{cool} = P_{cool}/V$, where $V = \frac{4}{3}\pi R^3$ is the volume of the sphere, can be estimated using (15). R is the radius of the sphere. The cooling power density for nanospheres with different radii in the range between 150 nm and 650 nm is plotted in Fig. 4. It changes considerably on this range and has several peaks. The radii of the nanospheres corresponding to these peaks are very close to the resonant radii of the Mie resonant modes.

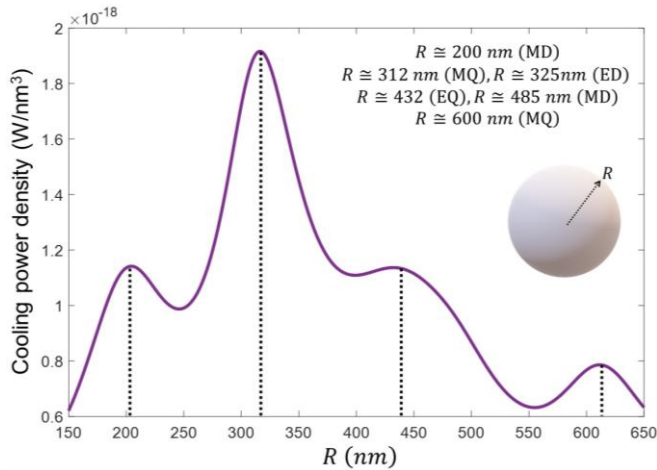


Fig. 4. Cooling power density generated in nanospheres with different radii. Resonant radii of the nanospheres supporting MD, ED, MQ, and EQ mode are presented for simplicity of understanding.

As may be seen in Fig. 4, the values of these peaks are different from each other. The largest peak corresponds to the radius $\sim 317 \text{ nm}$. The nanosphere with this radius can

support both the MQ and ED modes. The resonant radii for these modes ($\sim 312 \text{ nm}$ and $\sim 325 \text{ nm}$) are very close to the radius of the nanosphere $\sim 317 \text{ nm}$. If the radius of nanosphere is $\sim 200 \text{ nm}$, only the MD mode can be supported by the sample. If the radius of the nanosphere is equal to $\sim 430 \text{ nm}$ the peak is very broad, since one of the Mie resonant modes (the EQ mode) has the resonant radius, which is very close the radius of this peak, but the MD mode has the resonant radius $\sim 485 \text{ nm}$, which is essentially different from the radius of the nanosphere ($\sim 430 \text{ nm}$). This MD mode only weakly influence this peak. The peak corresponding to the nanosphere with the radius $\sim 612 \text{ nm}$ is small. It is located near the resonant radius of the MQ mode, which is $\sim 600 \text{ nm}$. There are no any other Mie modes with the resonant radii close to $\sim 612 \text{ nm}$.

With the knowledge of the cooling power density, it is possible to estimate the temperature of the nanospheres using relation (5). These results are presented in Fig. 5, which plots the temperature of the nanosphere, T_S , versus its radius in the same radius range between 150 nm and 650 nm as the cooling power density has been calculated in Fig. 4.

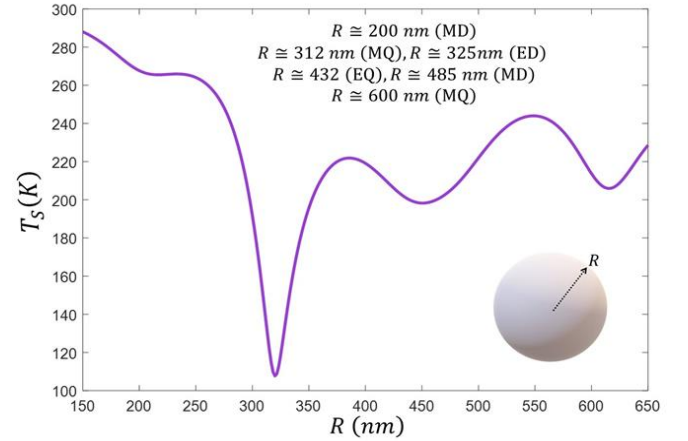


Fig. 5. Sample temperature, T_S , versus the radius of the sample. Resonant radii of the nanospheres supporting MD, ED, MQ, and EQ mode are presented for simplicity of understanding.

As one might expect, the radii of the nanospheres for which temperature reaches minima almost perfectly coincide with those associated with highest cooling power density (Fig. 4), the small discrepancy between the two being caused by the nonlinear relation between the cooling power and the temperature of the nanosphere (5), which for the spherical sample has the form $R\rho_{cool} = 3\varepsilon\sigma_B(T_r^4 - T_S^4)$. As is obvious from this relation, the radius of the nanosphere and the cooling power density generated in the nanosphere influence the drop in the temperature of the sample. The cooling power density generated in the nanospheres with the radii $\sim 200 \text{ nm}$ and $\sim 432 \text{ nm}$ are almost equal to each other (Fig. 4), but the temperature of the nanosphere with the radius $\sim 432 \text{ nm}$ exceeds the temperature of the nanosphere with the radius $\sim 200 \text{ nm}$ (Fig. 5). The minimal temperature in Fig. 5 is $T_S = 107 \text{ K}$. It can be reached if the radius of the nanosphere is equal to $\sim 320 \text{ nm}$. The temperature of this nanosphere drops

by $\sim 60\%$ of the temperature of the nanosphere ($T_S = 265\text{ K}$) with the radius $\sim 250\text{ nm}$; it drops by $\sim 63\%$ of the temperature of the nanosphere ($T_S = 288\text{ K}$) with the radius $\sim 150\text{ nm}$, and by $\sim 51\%$ of the temperature of the nanosphere ($T_S = 222\text{ K}$) with the radius $\sim 375\text{ nm}$. This considerable decrease in the temperature of the nanosphere at the radius $R = 320\text{ nm}$ is caused by the enhancement of the cooling power density in the sample which is itself caused by the ED and MQ Mie resonating modes.

IV. CONCLUSIONS

We have proposed to use Mie resonant modes to enhance laser cooling in RE-doped nanospheres made of low-phonon glasses or crystals. This concept has been comprehensively investigated for Yb^{3+} :YAG nanospheres with radii in the order of a few hundred nanometers. We have considered Yb^{3+} :YAG nanospheres pumped in the long-wavelength tail of the Yb^{3+} absorption spectrum at the wavelength $\lambda_p = 1030\text{ nm}$. We have shown a considerable enhancement of the cooling power density due to the Mie resonant modes and a related substantial ($\sim 60\%$) decrease in the temperature of the laser cooled samples with the radius $\sim 320\text{ nm}$. This sample supports MQ and ED Mie modes. A smaller decrease in the temperature of the laser cooled nanosphere is obtained if the sample supports only one Mie mode, as in the case of the Yb^{3+} :YAG nanospheres with the radii $\sim 200\text{ nm}$, $\sim 450\text{ nm}$, and $\sim 650\text{ nm}$. Nanospheres with the radii hundred nanometers are used widely in biophysics and mesoscopic physics.

As we already mentioned for samples of such a size scale, phonon quantization, which can influence the thermalization process, the change in the energy levels of the RE ions doped in the sample, as well as the Purcell effect, are not essential. Quantization becomes important only for spheres with smaller radii, in the order of a few nanometers. For such small sphere, quantization can dramatically enhance the laser cooling process, but the related technology becomes naturally challenging.

A lot of theoretical and experimental research is currently devoted to the laser cooling of nanoparticles. In the majority of the related work, only the translational energy of the particles has been suppressed. Removal of the internal energy embedded in the vibrational degrees of freedom of the particles, which has been considered in this work, remains an unsettled problem. Nowadays, laser cooling with anti-Stokes fluorescence is the only possible technique permitting to remove the internal energy of the sample, but the efficiency of this technique is very low (a few %). Our proposed approach based on the Mie resonant modes may therefore be considered as a timely new tool for experimentalists working on the laser cooling of solid nano-samples.

References

1. P. Pringsheim, Zwei Bemerkungen über den Unterschied von Lumineszenz- und Temperaturstrahlung, *Z. Phys.*, **57**, 739-746 (1929).
2. R. I. Epstein, M. I. Buchwald, B. C. Edwards, T. R. Gosnell and C. E. Mungan, Observation of laser-induced fluorescent cooling of a solid, *Nature (London)*, **377**, 500-502 (1995).
3. M. Sheik-Bahae, R. I. Epstein, Laser cooling of solids, *Laser Photon. Rev.* **3**, 67-84 (2009).
4. G. Nemova, R. Kashyap, Laser cooling of solids, *Rep. Prog. Phys.*, **73**, 086501:1-20 (2010).
5. D. V. Seletskiy, M. P. Hehlen, R. I. Epstein, M. Sheik-Bahae, Cryogenic optical refrigeration, *Adv. Opt. Photon.*, **4**, 78-107 (2012).
6. G. Nemova, *Field guide to laser cooling methods*, SPIE Press, Bellingham, Washington (2019).
7. S. Rostami, A. R. Albercht, M. R. Ghasemkhani, S. D. Melgaard, A. Gragossian, M. Tonelli, M. Sheik-Bahae, Optical refrigeration of Tm:YLF and Ho:YLF crystals, *Optical and Electronic Cooling of Solids*, **9765**:97650P (2016).
8. G. Nemova (ed), *Laser cooling: fundamental properties and application*, Pan Stanford Publishing, Singapore (2016).
9. S. D. Melgaard, D. V. Seletskiy, V. Polyak, Y. Asmerom, M. Sheik-Bahae, Identification of parasitic losses in Yb:YLF and prospects for optical refrigeration down to 80K, *Optics Express*, **22**, 7756-7764 (2014).
10. S. D. Melgaard, D. V. Seletskiy, A. Albrecht, M. Sheik-Bahae, First solid-state cooling below 100K, *SPIE Newsroom* (March 13, 2015). doi:10.1117/2.1201503.005790.
11. M. P. Hehlen, J. Meng, A. R. Albrecht, E. R. Lee, A. Gragossian, S. P. Love, C. E. Hamilton, R. I. Epstein, M. Sheik-Bahae, First demonstration of an all-solid-state optical cryocooler, *Light: Science & Applications*, **7**(15), 1-10 (2018).
12. S. R. Bowman, Laser without internal heat generation, *IEEE J. Quantum Electron.*, **35**, 115 (1999).
13. G. Nemova, R. Kashyap, Thin-disk athermal laser system, *Opt Commun*, **319**, 100-105 (2014).
14. Z. Yang, J. Meng, A. R. Albrecht, M. Sheik-Bahae, Radiation-balanced Yb:YAG disk laser, *Optics express*, **27** (2), 1392-1400 (2019).
15. G. Nemova, R. Kashyap, Fiber amplifier with integrated optical cooler, *J. Opt. Soc. Am. B*, **26**, 2237-2241 (2009).
16. E. Moboni, M. Peysokhan, A. Mafi, Heat mitigation of a core/cladding Yb-doped fiber amplifier using anti-Stokes fluorescence cooling, *J. Opt. Soc. Am. B*, **36**(8):2167 (2019).
17. X. Xia, A. Pant, J. Davis, P. J. Pauzauskie, Design of a radiation-balanced fiber laser via optically active composite cladding materials, *J. Opt. Soc. Am. B*, **36**(12):3307 (2019).
18. G. Nemova, R. Kashyap, Optimization of optical refrigeration in Yb^{3+} :YAG samples, *J. Lumin.*, **164**, 99-104 (2015).
19. S. S. Rudyi, T. A. Vovk, A. V. Kovalev, V. M. Polyakov, A. V. Ivanov, E. Y. Perlin, Y. V. Rozhdestvensky, Deep laser cooling of rare-earth-doped nanocrystals in a radio-

- frequency trap, *J. Opt. Soc. Am. B*, **34**(12), 2441-2445 (2017).
20. A. T. M. Anishur Rahman, P. F. Barker, Laser refrigeration, alignment and rotation of levitated Yb^{3+} :YLF nanocrystals, *Nature Photonics*, **11**, 634-638 (2017).
 21. P. B. Roder, B. E. Smith, X. Zhou, M. J. Crane, P. J. Pauzauskie, Laser refrigeration of hydrothermal nanocrystals in physiological media, *Proc. Natl. Acad. Sci. USA*, **112**, 15024-15029 (2015).
 22. G. Mie, Beitrage zur Optik truber Medien, speziell kolloidaler Metallosungen, *Ann. Phys.* **330**, 377-445 (1908).
 23. E. Soares de Lima Filho, G. Nemova, S. Loranger, R. Kashyap, Ytterbium-doped glass-ceramics for optical refrigeration, *Opt. Express*, **23**(4), 4630-4640 (2015).
 24. C. F. Bohren, D. R. Huffman, Absorption and scattering of light by small particles. WILEY-VCH Verlag GmbH & Co. KGaA, Weinheim (2004).